Magnetoresistance of a Permalloy Single Crystal and Effect of 3d Orbital Degeneracies*

L. BERGER AND S. A. FRIEDBERG
Department of Physics, Carnegie Institute of Technology, Pittsburgh, Pennsylvania
(Received 8 May 1967)

The electrical resistance of single crystals of the alloy 15% Fe-85% Ni has been measured at 20, 77, and 299°K, in a transverse or longitudinal magnetic field sufficient to cause ferromagnetic saturation. The current is parallel to a ⟨100⟩, ⟨110⟩, or ⟨111⟩ direction. At 20°K, a change in orientation of the magnetization causes changes of resistivity reaching 30%. The temperature variation of the phenomenological Döring coefficients k_1–k_5 follows largely from their dependence on the type of scattering centers; the coefficients are large and positive in the case of impurity scattering alone, and are small or slightly negative in the case of phonon or magnon scattering alone. A microscopic theory has also been developed according to which conduction electrons are scattered by impurities into near-degenerate 3d states; these states are strongly perturbed and mixed by the interaction AL_zS_z. The perturbation of a near-degenerate pair of states is found to be highly anisotropic, and is possible only along a certain "polarization axis." Two different models reproduce correctly most features of the experimental data and are consistent with cubic symmetry. In the first model, the polarization axes are assumed to be parallel to the fourfold cubic axes of the crystal, and spin-orbit perturbation is assumed to decrease the probability of being scattered into a state of the pair. In the other model, the polarization axes are along the threefold cubic axes, and spin-orbit interaction increases the scattering probability. In both models, it is necessary to assume that the spin-orbit perturbation of a pair is large and nonlinear (because of the near degeneracy), in such a way that it tends to saturate at an almost constant value. Calculations of impurity scattering are made in the Slater-Koster approximation. The theory is then extended to show that the validity and success of these two models is actually independent of whether the AL_zS_z interaction or the $A(L_xS_x+L_yS_y)$ interaction is the perturbing agent.

I. INTRODUCTION

THE electrical resistance of nickel single crystals,[1–5] or of iron single crystals,[1,6–9] in an external magnetic field has been measured by several authors. Similar data exist in the case of dilute Fe–Si alloys,[8,10] of the alloy[4] 60% Ni–40% Fe, and of Cu–Ni alloy films.[11] The magnetoresistance effects observed at room temperature or in alloys are probably due[12–15] to the spin-orbit interaction influencing the scattering mechanisms. On the other hand, the effects observed at very low temperature in very pure nickel, iron, or cobalt,[5,9,12,13,15,16] are due to the Lorentz force, or to scattering by domain walls, and will not be considered here.

Electrical resistivity measurements[12,15] on polycrystalline Fe–Ni and Co–Ni alloys corresponding to an electron concentration of 27.7 electrons per atom show very large effects of spin-orbit interaction. These large effects are also present in measurements of the thermal conductivity of Fe–Ni alloys.[15] They are probably due to the presence of an orbital degeneracy at the Fermi level of the alloy.[13]

The present single-crystal measurements are a tool to study the perturbation of 3d states by spin-orbit interaction. This method provides a very narrow energy window, looking selectively at states located at the Fermi level. From that point of view, the analysis of measurements of other quantities depending on spin-orbit interaction, such as the magnetocrystalline anisotropy or the gyromagnetic ratio, is not so simple since all states below the Fermi level contribute in that case.

II. DESCRIPTION OF SAMPLES AND OF APPARATUS

A single crystal of the alloy 15% Fe–85% Ni, obtained by one pass of zone-melting, was purchased from Materials Research Corporation, Orangeburg, New York. The crystal was then deeply etched in aqua regia, to reveal the etch pits used for orientation. The optical reflections are mainly on {111} planes, as in pure nickel.[17] Small rods with a cross-section area of about 1mm square were cut from the crystal, using a diamond wheel and a slow motor-driven watchmaker's blade saw. The rods were ground to an octagonal cross section with a wet, fine-grained, carborundum

* Work supported by the U.S. Army Research Office (Durham) and by the U.S. Office of Naval Research.
[1] W. L. Webster, Proc. Phys. Soc. (London) **42**, 431 (1930).
[2] S. Kaya, Sci. Rept. Tohoku Univ. **17**, 1027 (1928).
[3] W. Döring, Ann. Physik **32**, 259 (1938).
[4] V. Marsocci, J. Appl. Phys. **35**, 774 (1964).
[5] E. Fawcett and W. A. Reed, Phys. Rev. Letters **9**, 336 (1962).
[6] W. L. Webster, Proc. Roy. Soc. (London) **A113**, 196 (1926); **A114**, 611 (1927).
[7] Y. Shirakawa, Sci. Rept. Tohoku Univ. **29**, 132 (1940); **29**, 152 (1940); T. Hirone and N. Hori, *ibid.*, First Ser., **30**, 125 (1942); Y. Gondo and Z. Funatogawa, J. Phys. Soc. Japan **7**, 41 (1952).
[8] E. Tatsumoto, Phys. Rev. **109**, 658 (1958).
[9] W. A. Reed and E. Fawcett, Phys. Rev. **136**, A422 (1964); A. Isin and R. V. Coleman, *ibid.* **137**, A1609 (1965); **142**, 372 (1966); E. E. Semenenko and A. I. Sudovtsov, Zh. Eksperim. i Teor. Fiz. **47**, 486 (1964) [English transl.: Soviet Phys.—JETP **20**, 323 (1965)].
[10] R. Parker, Proc. Phys. Soc. (London) **B63**, 996 (1950).
[11] R. H. Walden and R. F. Cotellessa, J. Appl. Phys. **38**, 1335 (1967).
[12] J. Smit, Physica **17**, 612 (1951).
[13] L. Berger, Physica **30**, 1141 (1964).
[14] J. Kondo, Progr. Theoret. Phys. (Kyoto) **27**, 772 (1962).
[15] L. Berger and D. Rivier, Helv. Phys. Acta **35**, 715 (1962).
[16] L. Berger and A. R. De Vroomen, J. Appl. Phys. **36**, 2777 (1965).
[17] J. G. Walker, H. J. Williams, and R. M. Bozorth, Rev. Sci. Instr. **20**, 947 (1949).

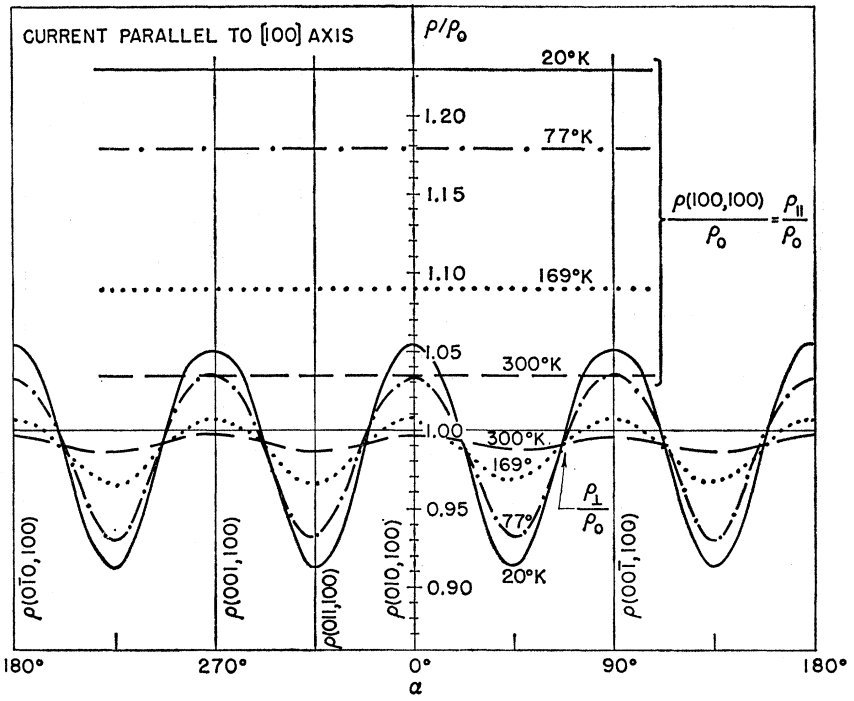

FIG. 1. Resistivity of a ⟨100⟩ sample in a transverse or longitudinal field, relative to the zero-field resistivity ρ_0. The angle of the transverse field with a [010] crystal direction is called α. $\rho(001, 100)$ means that the magnetic field is along [001], and the current along [100].

wheel, and then rolled between two pieces of emery cloth until a circular cross section was obtained. Care was exercised in order to apply only moderate stresses. Finally, the samples were etched in aqua regia, to remove the surface layers. No thermal treatment was used.

Of the three samples which have been investigated, the first one has an axis parallel to a ⟨100⟩ direction, the second parallel to a ⟨110⟩ direction, and the third one parallel to a ⟨111⟩ direction. These crystal orientations were checked[17] by x-ray reflections, and found to be correct to better than ±5°. The diameter is close to 0.8 mm, and the length close to 5 mm. Copper wires were soft-soldered to the ends, as current leads. The edges of two thin phosphor bronze strips were pressed against the sample as potential probes, 2.5 mm apart. The difference of potential is directly recorded by a Brown Electronik automatic potentiometer, with a full-scale deflection corresponding to 1 mV. The sample current is between 1 and 5 A.

Though the sample geometry is not defined with enough accuracy to allow an accurate determination of the absolute resistivity, the values $\rho = 14\text{–}15 \times 10^{-8}$ Ωm found at 300°K seem compatible with the data of the literature.[18] The resistivity ratio $\rho_{299}/\rho_{4.2}$ was equal to 4.16±0.04 for each of the three samples. This is larger than the value $\rho_{293}/\rho_{4.2} = 3.50$ found[15] for a polycrystalline sample of the same alloy. Even though the alloy differs considerably from the composition Ni_3Fe most favorable to the formation of a superlattice, the possibility of some degree of ordering cannot be completely excluded.

A chemical analysis performed by Schwarzkopf Microanalytical Laboratory, Woodside, New York, on fragments of the single crystal gave a composition of 85.4% Ni±0.5% and 13.9% Fe±0.5% in mass.

III. EXPERIMENTAL RESULTS

Figure 1 shows the relative values of the resistivity $\rho_\perp$ of the ⟨100⟩ sample, in a transverse external field of 8000 G. The sample is rotated slowly around its axis by a synchronous motor. The resistivity $\rho_{||}$ in a longitudinal external field of 940 G is shown by horizontal lines on the upper part of the same diagram. All values are relative to the zero-field resistivity ρ_0 at the same temperature. When we write $\rho(001, 100)$, 001 refers to the magnetic field direction, and 100 refers to the current direction.

The results for the ⟨110⟩ sample are shown in Fig. 2. The average transverse resistivity and the longitudinal resistivity for the ⟨111⟩ sample are given in Table I. In this last case the transverse rotation pattern did not have the expected sixfold symmetry; this may be due to the sixfold resistance variations being small and easily masked by small crystal orientation errors.

The fields were sufficient to cause ferromagnetic saturation, but small enough that a correction for the effect of the slope of the resistance above saturation is not necessary.

The measurements are performed at 20, 77, and in a bath of light oil at 299°K±2°. In the case of the ⟨100⟩

[18] R. Bozorth, *Ferromagnetism* (D. Van Nostrand Company, Inc., Princeton, New Jersey, 1951), p. 107.

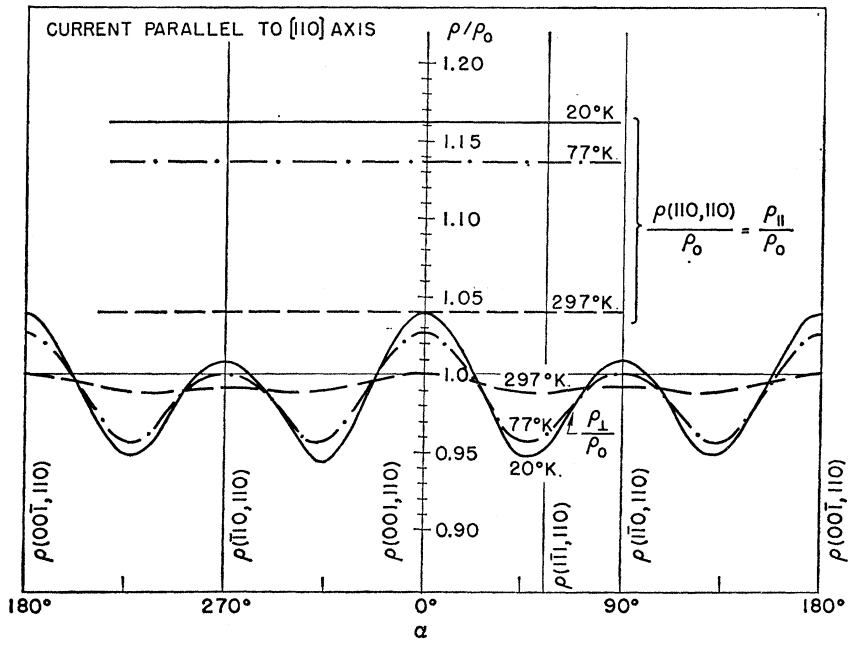

FIG. 2. Resistivity of a ⟨110⟩ sample in a transverse or longitudinal field, relative to the zero-field resistivity ρ_0. The angle of the transverse field with a [001] crystal direction is called α.

sample, they are done at 169°K, too, in a bath of liquid ethylene.

The relative values of the zero-field resistivity ρ_0 at various temperatures are given in Table II. This includes one zero-field measurement done at 4.2°K in liquid helium on the ⟨110⟩ sample.

IV. DERIVATION OF THE DÖRING COEFFICIENTS

Döring[3] has given a general expression for the resistivity of a saturated ferromagnetic cubic single crystal, correct up to fourth order in the components of the magnetization:

$$\rho/\rho_0=1+\delta+k_1(\alpha_1^2\beta_1^2+\alpha_2^2\beta_2^2+\alpha_3^2\beta_3^2-\tfrac{1}{3})$$
$$+k_2(2\alpha_1\alpha_2\beta_1\beta_2+2\alpha_2\alpha_3\beta_2\beta_3+2\alpha_3\alpha_1\beta_3\beta_1)+k_3(s-\tfrac{1}{3})$$
$$+k_4(\alpha_1^4\beta_1^2+\alpha_2^4\beta_2^2+\alpha_3^4\beta_3^2+\tfrac{2}{3}s-\tfrac{1}{3})$$
$$+k_5(2\alpha_1\alpha_2\alpha_3^2\beta_1\beta_2+2\alpha_2\alpha_3\alpha_1^2\beta_2\beta_3+2\alpha_3\alpha_1\alpha_2^2\beta_3\beta_1);$$
$$(s=\alpha_1^2\alpha_2^2+\alpha_2^2\alpha_3^2+\alpha_3^2\alpha_1^2), \quad (1)$$

where α_1, α_2, and α_3 are the components of the unit vector α parallel to the saturation magnetization, and where β_1, β_2, and β_3 are the components of the unit vector β parallel to the current. The coefficient δ vanishes if the easy directions are ⟨111⟩, and if they are equally populated in the zero-field state.

Using a digital computer, we have fitted Eq. (1) to the data of Figs. 1 and 2, and Table I. The best values of k_1–k_5 are given in Table III. Neither the zero-field state nor δ are reproducible, and it is advisable to leave δ out of the fitting process by considering only resistivity differences.

In Table IV, the Döring coefficients of pure nickel[3] and of pure iron[7] at room temperature are given for the sake of comparison. In the range 20–300°K which has been investigated, our alloy is similar to pure nickel, in the sense that the measured values of k_3 and k_4 are negative, and that k_1 is larger than k_2.

In the case of alloy polycrystals, Parker[15,19] has suggested that most of the thermal variation of the magnetoresistance is due to the change from impurity to phonon (or magnon) scattering. Let us write Matthiessen's rule for the resistivity, in the case of two different orientations 1 and 2 of the saturation magneti-

TABLE I. Resistivity $\rho_\perp$ of a ⟨111⟩ sample in a transverse field, averaged over all possible directions of that field. Resistance $\rho_{||}$ in a longitudinal field.

T(°K)	$\rho_\perp/\rho_0$	$\rho_{||}/\rho_0$
20	1.006	1.193
77	1.004	1.1595
299±2	0.997	1.047

TABLE II. Values of the zero-field resistivity ρ_0 at temperature T, relative to the value at 20°K.

T(°K)	⟨100⟩ sample	⟨110⟩ sample	⟨111⟩ sample
4.2	...	0.942	...
77	1.21	1.24	1.20
169	2.03	...	...
299±2	3.96	3.92	3.88

[19] R. Parker, Proc. Phys. Soc. (London) **A64**, 447 (1951); **B64**, 930 (1951); **B65**, 616 (1952).

TABLE III. The Döring coefficients k_1, k_2, k_3, k_4, k_5, of a 15% Fe–85% Ni single crystal.

T(°K)	k_1	k_2	k_3	k_4	k_5	$(\rho_0)_{ph}/\rho_0 = (\rho_0(T)-\rho_0(4.2))/\rho_0(T)$
20	0.549	0.144	−0.263	−0.378	0.247	0.058
77	0.409	0.131	−0.195	−0.264	0.170	0.215
299±2	0.0518	0.0478	−0.0243	−0.0139	0.0259	0.760

zation (or of the current) and also for the zero-field case 0:

$$\rho_1=(\rho_1)_{imp}+(\rho_1)_{ph},$$
$$\rho_2=(\rho_2)_{imp}+(\rho_2)_{ph},$$
$$\rho_0=(\rho_0)_{imp}+(\rho_0)_{ph}. \quad (2)$$

Then

$$\frac{\rho_2-\rho_1}{\rho_0}$$
$$=\frac{(\rho_0)_{imp}}{\rho_0}\left[\frac{\rho_2-\rho_1}{\rho_0}\right]_{imp}+\frac{(\rho_0)_{ph}}{\rho_0}\left[\frac{\rho_2-\rho_1}{\rho_0}\right]_{ph} \quad (3a)$$
$$=\frac{(\rho_0)_{ph}}{\rho_0}\left(\left[\frac{\rho_2-\rho_1}{\rho_0}\right]_{ph}-\left[\frac{\rho_2-\rho_1}{\rho_0}\right]_{imp}\right)+\left[\frac{\rho_2-\rho_1}{\rho_0}\right]_{imp}, \quad (3b)$$

where $[(\rho_2-\rho_1)/\rho_0]_{imp}$ and $[(\rho_2-\rho_1)/\rho_0]_{ph}$ are constants representing the values that $(\rho_2-\rho_1)/\rho_0$ would have if, respectively, impurity scattering or phonon scattering were acting alone. In Eq. (3b), the ratio $[(\rho_2-\rho_1)/\rho_0]_{ph}$ is independent of the number of phonons present per unit volume, since both numerator and denominator are proportional to that number. The ratio might depend on the characteristics of a phonon, such as the average wavelength, etc., but these are constant at the Debye temperature and above. As a result, $[(\rho_2-\rho_1)/\rho_0]_{ph}$ is independent of temperature, except possibly at temperatures considerably below the Debye temperature. Of course, this argument may not hold so well if magnons contribute appreciably to electron scattering, since their wavelength is temperature-dependent.

Then, when using Eq. (3b), we assume that only $(\rho_0)_{ph}/\rho_0$ depends on temperature; it is calculated in Table III from Table II. Parker has also introduced an empirical correction to take into account the influence of the thermal decrease of the saturation magnetization, but this is negligible for our alloy at room temperature and below.

Because the Döring coefficients of an alloy single crystal are related linearly to differences in the resistivity measured at various α or β directions, one would expect them to obey an equation similar to Eq. (3b), that is, to vary with temperature as a linear function of $(\rho_0)_{ph}/\rho_0$. Figure 3, which uses the data of Table III, suggests that this is verified only approximately. The intercepts of the extrapolated straight lines on the right side or left side vertical axis give, respectively, the values of the Döring coefficients for phonon scattering alone, and for impurity scattering alone. The first ones are found to be small or negative, while the second ones are large and positive. The departures from a straight line may be due to the phonon wavelength variations mentioned above.

V. QUANTUM THEORY OF THE FERROMAGNETIC ANISOTROPY OF RESISTIVITY

The magnetoresistance of ferromagnets is often called ferromagnetic anisotropy of resistivity. In 1951, Smit[12] proposed a mechanism for this anisotropy. The spin-flip part $A(L_xS_x+L_yS_y)$ of periodic spin-orbit interaction slightly admixes spin-down $3d$ states into nominally spin-up $3d$ states. Then it becomes possible for $4s$ spin-down conduction electrons to be scattered by impurities into these spin-up $3d$ states. For a given spin orientation, the degree of admixture is found to be different for the five $3d$ orbitals of various spatial orientation symmetries. Therefore, the scattering probability, as computed by the Born approximation, will depend on the angle between the k vector of the incident $4s$ conduction electron and the spin, resulting in the anisotropy of resistivity.

On the other hand, Berger[13] has used the non-flip Hamiltonian AL_zS_z. As before, this perturbation mixes the $3d$ states together in a way which lacks cubic symmetry; an anisotropy of the impurity scattering cross section and of the electrical-resistivity results. We will see that it is necessary to use here a better scattering approximation than the Born approximation. It is well known that this same AL_zS_z is responsible for the anomaly of the gyromagnetic ratio, and for the extraor-

TABLE IV. The Döring coefficients of pure nickel and of pure iron at room temperature, according to various authors.

	k_1	k_2	k_3	k_4	k_5
Nickel (Döring[a])	0.0654	0.0266	−0.032	−0.054	0.020
Iron (Hirone and Hori[b])	0.00153	0.00593	0.00194	−0.00053	−0.00269

[a] Reference 3. [b] Reference 7.

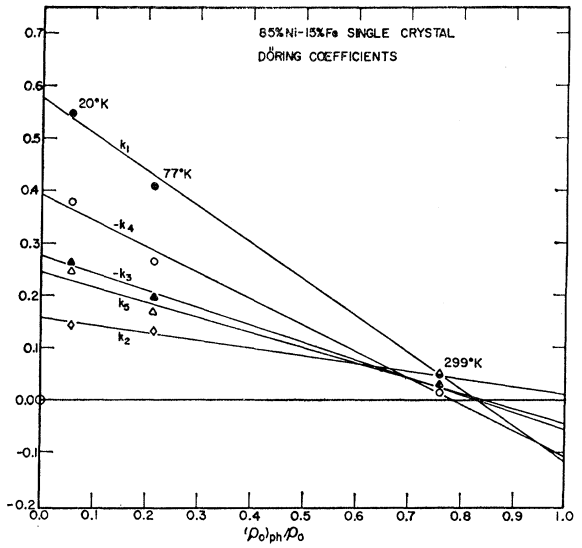

FIG. 3. The Döring coefficients at 20, 77, and 299°K, plotted against $(\rho_0)_{ph}/\rho_0=(\rho_0(T)-\rho_0(4.2))/\rho_0(T)$. The signs of k_3 and k_4 have been changed to make them positive.

dinary Hall effect R_s; therefore, using the present mechanism, it has been possible[13] to explain the relation between the singularities of the anisotropy and of R_s observed in series of Fe–Ni and Co–Ni alloys, by introducing the assumption that a near degeneracy is present in the 3*d* band structure close to the Fermi level of the alloy. The same assumption explains[20] the change of sign of the magnetostriction in the same alloy series.

Using the full spin-orbit Hamiltonian $A(L_xS_x+L_yS_y+L_zS_z)$, Kondo[14] calculated the anisotropy of resistivity in the case of magnon scattering. However, our Fig. 3 shows that impurity scattering is the main cause of anisotropy in our alloy, and we will not consider magnon or phonon scattering any further.

VI. CASE OF SINGLE CRYSTALS

We can hope that the theories mentioned in Sec. V give a qualitative explanation of the anisotropy observed in polycrystals. However, there remains to give an explanation of more detailed experiments performed on cubic single crystals, which have been summarized in our orientation diagrams of Figs. 1 and 2, in Table I, or in the values of the Döring coefficients of Table III.

Marsocci[21] has used Smit's theory with $A(L_xS_x+L_yS_y)$ to calculate an orientation diagram for single-crystal films of nickel and of an iron-nickel alloy. The current was assumed to be parallel to a ⟨100⟩ direction. However, since he takes into account all five 3*d* orbitals of a given spin and, like Smit, assumes them to be all degenerate, there is no way in which the cubic symmetry of the crystal can actually be felt by the 3*d* electrons in his model, and his result (see solid circles in his Fig. 1) must be due to some error, presumably the neglect of interference terms between the probability amplitudes for the various scattered 3*d* states. This is also indicated by the fact that the (arbitrary) *Oz* quantization axis appears as a privileged direction in his theoretical curve. Nevertheless, there is little doubt that Smit's theory could be used if certain types of 3*d* orbitals were assumed to dominate over others. This will be sketched at the end of the present paper.

We will now try to use the other theory.[13] The first problem is to calculate the effect of AL_zS_z on the band structure, with certain simplifying assumptions. The second problem involves the calculation of cross sections for impurity scattering, and of the electrical resistivity.

VII. ORBITAL MAGNETIC POLARIZATION OF A PAIR OF STATES

As in our original paper,[13] we assume that a pair of nearly degenerate orbital states ψ_a and ψ_b with parallel spins is present in the 3*d* band of the alloy. Their spin, for example, is parallel to the saturation magnetization (spin-up).

They are mixed together by $AL_z'S_z'$, where the $0x'y'z'$ system is defined such that the z' axis is always along the saturation magnetization.

$$\psi=a\psi_a+b\psi_b. \tag{4}$$

The unit vector $\boldsymbol{\alpha}$ parallel to the saturation magnetization has the components α_1, α_2, and α_3 relative to the fourfold axes $0xyz$ of the crystal,

$$L_z'=\alpha_1L_x+\alpha_2L_y+\alpha_3L_z.$$

Let us introduce a real-valued vector $\mathbf{m}$ by its components in the $0xyz$ system:

$$\begin{aligned} m_1&=i^{-1}\langle\psi_a\,|\,L_x\,|\,\psi_b\rangle;\\ m_2&=i^{-1}\langle\psi_a\,|\,L_y\,|\,\psi_b\rangle;\\ m_3&=i^{-1}\langle\psi_a\,|\,L_z\,|\,\psi_b\rangle. \end{aligned} \tag{5}$$

Then, for spin-up electrons,

$$\begin{aligned} \langle\psi_a\,|\,AL_z'S_z'\,|\,\psi_b\rangle&=A\langle\psi_a\,|\,S_z'\,|\,\psi_b\rangle i(\alpha_1m_1+\alpha_2m_2+\alpha_3m_3)\\ &=\tfrac{1}{2}(iA\hbar)\,\boldsymbol{\alpha}\cdot\mathbf{m}. \end{aligned} \tag{6}$$

Moreover, because of parity and time-reversal invariance, the diagonal matrix elements of $AL_z'S_z'$ vanish. Equation (6) shows, therefore, that the degree of mixing of the two 3*d* states by spin-orbit interaction depends only on the component of the magnetization along a certain fixed vector $\mathbf{m}$. Conversely, the states ψ of Eq. (4), with arbitrary coefficient a and b, have $\langle\mathbf{L}\rangle$ always parallel or antiparallel to $\mathbf{m}$. The maximum possible $\langle\mathbf{L}\rangle$ expectation is in fact $\pm\mathbf{m}$, and is obtained when $a=\pm ib$. We call $\mathbf{m}$ the "orbital magnetic vector" of the pair ψ_a, ψ_b.

VIII. DELTA MODEL FOR THE 3*d* STATES

We assume the 3*d* states to be itinerant and described by the tight-binding approximation. The

[20] L. Berger, Phys. Rev. **138**, A1083 (1965).
[21] V. Marsocci, Phys. Rev. **137**, A1842 (1965).

periodic $AL_z'S_z'$ mixes together only states of the same $\mathbf{k}$.

Then one has to specify the direction of $\mathbf{m}$ for each point of the $3d$ Fermi surface where near-degenerate pairs exist. We assume that, due to crystal field and band splittings, certain types of pairs and correspondingly certain $\mathbf{m}$ directions are dominant at the Fermi level over other types.

We first investigate a model in which the dominant degenerate pairs are of three different kinds, numbered by the subscript j, each of them associated with one of the three fourfold cubic axes and having its orbital magnetic vector $\mathbf{m}_j$ along this axis (Fig. 4). This "delta model" is consistent with cubic symmetry and is similar to the assumption made for the case of polycrystals in our former paper.[13] These three kinds of pairs are perhaps associated with portions of the $3d$ Fermi surface close to the fourfold axes in k space.

IX. IMPURITY SCATTERING IN THE PRESENCE OF SPIN-ORBIT INTERACTION

We assume[13] that the current carriers are $4s$ electrons and that these conduction electrons are scattered by impurities into vacant $3d$ states at the Fermi level. The net current carried by $3d$ electrons is neglected. These specific assumptions are not really necessary, and the present theory may well be valid under more general conditions.

The transition rates from one $4s$ state to the various regions of the $3d$ Fermi surface are additive, so that we assume for the symmetric resistivity tensor s_{ik}

$$s_{ik}=\sum_{j=1}^{3}(s_j)_{ik}+(s_b)_{ik}, \tag{7a}$$

where the "partial resistivity tensors" $(s_j)_{ik}$ correspond to the case where only transitions to $3d$ states belonging to one of the three dominant types (see Fig. 4) would be allowed. On the other hand, $(s_b)_{ik}$ is caused by transitions to a general background of other $3d$ states, assumed to be without pronounced features and to have over-all spherical symmetry. The only effect of this background is to dilute somewhat the strong crystal anisotropy effects introduced by the $(s_j)_{ik}$ terms. Equation 7a is remotely similar to Matthiessen's rule, and is subject to similar limitations.

By symmetry, one principal axis of $(s_j)_{ik}$ is parallel to $\mathbf{m}_j$; the two other axes are perpendicular to $\mathbf{m}_j$, and

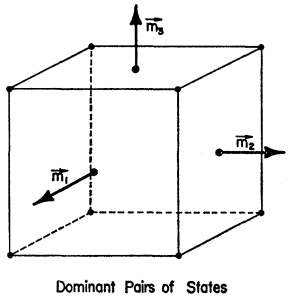

FIG. 4. Directions of the orbital magnetic axes $\mathbf{m}_j$ of dominant degenerate pairs ($j=1, 2, 3$), in the delta model.

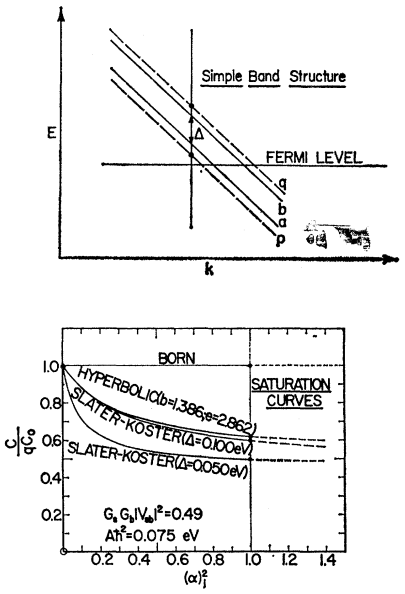

FIG. 5. "Saturation curves" describing the dependence of C on the square of the component of the unit magnetization vector $\boldsymbol{\alpha}$ along $\mathbf{m}_j$. Scattering is calculated by the Slater–Koster approximation or by the first Born approximation. The curve marked "hyperbolic" corresponds to the empirical analytical expression of Eq. (10), for $b=1.386$, $e=2.862$. The assumed band model is shown above, the curves a and b corresponding to the absence of spin-orbit interaction. Scale on E and k axes is arbitrary, since the C/qC_0 value calculated from this band model depends on Δ but not on the common slope of a and b.

correspond to equal eigenvalues;

$$(s_j)_{ik}=2C(\delta_{ik}-(p/|\mathbf{m}|^2)(\mathbf{m}_j)_i(\mathbf{m}_j)_k), \qquad (p<1) \tag{7b}$$

where $(m_j)_i$ represents a component of $\mathbf{m}_j$ in the $0xyz$ system.

Since the background favors no special crystal direction, we must have, as in a polycrystal,

$$(s_b)_{ik}=C_0(\delta_{ik}+A_2\alpha_i\alpha_k). \tag{7c}$$

X. SATURATION CURVE

The tensor $(s_j)_{ik}$ may depend on the mixing of $3d$ states constituting a pair, and therefore, by Eq. (6), on the component of $\boldsymbol{\alpha}$ along $\mathbf{m}_j$, which we call $(\alpha)_j$,

$$(\alpha)_j=\boldsymbol{\alpha}\cdot\mathbf{m}_j/|\mathbf{m}_j|, \qquad (-1\leq(\alpha)_j\leq 1) \tag{8}$$

The exact form of the dependence may vary with the model used to describe impurity scattering. However, in all cases, the following important facts hold:

(a) $(s_j)_{ik}$ is an even function of $(\alpha)_j$, and depends only on $(\alpha)_j^2$.

(b) For small values of $(\alpha)_j^2$, the elements of $(s_j)_{ik}$ depend linearly on $(\alpha)_j^2$.

(c) For large values of $(\alpha)_j^2$, the mixing between states of the pair by the interaction $AL_z'S_z'$, is almost complete ($a\approx\pm ib$), and becomes almost independent of $(\alpha)_j^2$. As a result, the elements of the tensor $(s_j)_{ik}$ tend to "saturate" at values independent of $(\alpha)_j^2$.

As a rough simplifying assumption, we assume that all elements vary in the same ratio; then p is independent of $(\alpha)_j^2$, and only C varies [see Eq. (7b)]. This agrees with a detailed numerical calculation made with the Slater-Koster approximation (described below). In the case of other scattering approximations, the assumption is probably at least qualitatively correct, in the sense that all elements go simultaneously up, or simultaneously down.

To provide one example of saturation behavior we have considered a near-degenerate $3d$ band (Fig. 5) consisting of two parallel branches a and b, separated by an energy Δ in the absence of spin-orbit interaction. The scattering of $4s$ electrons into $3d$ states by a very localized impurity potential is treated in the Slater-Koster[22] formalism, neglecting any matrix element of V between overlapping Wannier functions centered on different atoms. An expression for the s-d scattering rate is given by Gomes[23] in this approximation. In our case, considering separately the scattering into each of the two branches p and q which result from the mixing of branches a and b (Fig. 5), the total s-d scattering rate becomes

$$\tau^{-1}=\frac{2\pi}{\hbar}\frac{|b_p|^2|V_{sb}|^2 n_p}{|1-|b_p|^2 G_s G_p|V_{sb}|^2|^2}+\frac{2\pi}{\hbar}\frac{|b_q|^2|V_{sb}|^2 n_q}{|1-|b_q|^2 G_s G_q|V_{sb}|^2|^2} \quad (9)$$

if we assume $V_{sb}\neq V_{sa}=V_{ss}=0$. Since $A\hbar^2$ is much smaller than the bandwidth, the Green functions G_p and G_q for branches p and q at the Fermi level are affected very little by mixing, and we have $G_p\approx G_q\approx G_a\approx G_b$. The $3d$ densities of states $n_p=n_q$ are here exactly independent of mixing. It is through the coefficients b_p and b_q [see Eq. (4)] that mixing affects the scattering rate; they can be calculated by degenerate perturbation theory for any given value of $(\alpha)_j^2$, using Eq. (6). We assume $A\hbar^2=0.075$ eV, and $|\mathbf{m}|=2\hbar$. By Eq. (7b), C is proportional to the scattering rate. Hence the dependence of C on $(\alpha)_j^2$ may be calculated by Eq. (9), using a digital computer. The result (saturation curve) is shown on Fig. 5 for the cases $\Delta=0.050$ eV and $\Delta=0.100$ eV assuming $G_sG_b|V_{sb}|^2=0.49$. As could be expected, the larger Δ, the more linear is the saturation curve. The assumptions made in this Slater-Koster approximation may not be realistic, but the only purpose of the calculation is to give one simple example of saturation curve.

As long as we neglect overlap effects, this Slater-Koster approximation gives a scattering rate independent of $\mathbf{k}$ direction, for the incident $4s$ electron. This implies $p=0$ in Eq. (7b), in fortuitous agreement with the small value $p=0.0528$ obtained below by fitting to the experimental data.

With the same simple model of $3d$ band structure (Fig. 5) mentioned above, we have also solved the scattering problem by the first Born approximation. As shown in Fig. 5, the parameter C is then found to be independent of mixing, and is therefore independent of $(\alpha)_j^2$. The Born approximation is therefore inadequate[24] for our problem. More generally, if V is the strength of the impurity potential, and if the scattering rate varies like V^n, then mixing will decrease C for $n>2$, and increase C for $n<2$. We may have $n>2$ for our nickel-rich Ni–Fe alloy, since a replacement of Fe by stronger-scattering Cr or V atoms is known to lead to a $3d$ scattering resonance.

XI. CALCULATIONS WITH A HYPERBOLIC SATURATION CURVE

Instead of the saturation curve coming from the Slater-Koster approximation, we actually use in further numerical computations a similar curve having a much simpler analytical expression ("hyperbolic" saturation curve, see Fig. 5);

$$C=qC_0[1+b(\alpha)_j^2]/[1+e(\alpha)_j^2], \quad (10)$$

where q, b, and e are adjustable parameters. The value of q only determines in what proportion the special $3d$ states [Eq. (7b)] and the background [Eq. (7c)] contribute to the total resistivity.

Using Eqs. (7), (8), and (10), it is then possible, in the delta model, to compute the observed resistivity ρ, given by

$$\rho(\boldsymbol{\alpha},\boldsymbol{\beta})=\sum_i\sum_k s_{ik}\beta_i\beta_k. \quad (11)$$

With the help of a digital computer, the values of p, q, b, and e may be adjusted to fit the experimental rotation diagrams at 20°K, where impurity scattering is dominant. The value of C_0 is irrelevant, since we fit $\rho_{\parallel}/\rho_0$ and $\rho_{\perp}/\rho_0$ rather than absolute resistivity values. For ρ_0 we take the calculated resistivity value when $\boldsymbol{\alpha}\,||\,\langle 111\rangle$, $\boldsymbol{\beta}\,||\,\langle 100\rangle$.

The values of the parameters giving the best fit with the delta model are shown on the first line of Table V. The result of the fit is shown by the dashed curve in Figs. 6 and 7 in the case of a current parallel to a $\langle 100\rangle$ or $\langle 110\rangle$ direction; the solid curve is experimental. Finally, when the current is along $\langle 111\rangle$, the average $(\rho_{\parallel}-\rho_{\perp})/\rho_0$ is predicted to be $+0.145$, while the experimental value at 20°K (Table I) is $+0.187$.

We see that our delta model is able to reproduce correctly most qualitative features of the experimental data. Note that the results for both $\rho_{\parallel}/\rho_0$ and $\rho_{\perp}/\rho_0$ are represented on the same graphs. Even better agreement is obtained with the lambda model described below.

The curves obtained by fitting the Döring phenomenological theory to the data at 20°K (see coefficients in

[22] G. F. Koster, Phys. Rev. **95**, 1436 (1954).
[23] A. A. Gomes, J. Phys. Chem. Solids **27**, 451 (1966).

[24] Because of a computation error, it was incorrectly stated in our former publication (ref. 13) that the first Born approximation can be used for this problem. For the same reason, the curves in Fig. 10 of that paper are incorrect. Since that time, we have computed these curves again, using the Slater–Koster approximation. The curves then remain on one side of the horizontal axis and are in better agreement with the experimental data.

TABLE V. Values of parameters giving best fit of microscopic theory to the data at 20°K. Last column indicates average difference remaining between theory and experiment, in arbitrary units.

Interaction	Model	p	q	A_2	b	e	b'	e'	rms error
$AL_x'S_x'$	Delta	0.0528	0.8098	0.8882	1.386	2.862	···	···	0.0377
	Lambda	0.03950	0.5903	1.8206	4.758	1.117	···	···	0.0287
$A(L_x'S_x'+L_y'S_y')$	Delta	0.06306	0.8788	0.8557	···	···	1.246	2.971	0.0270
	Lambda	0.1709	0.5723	2.050	···	···	5.180	0.9031	0.0456

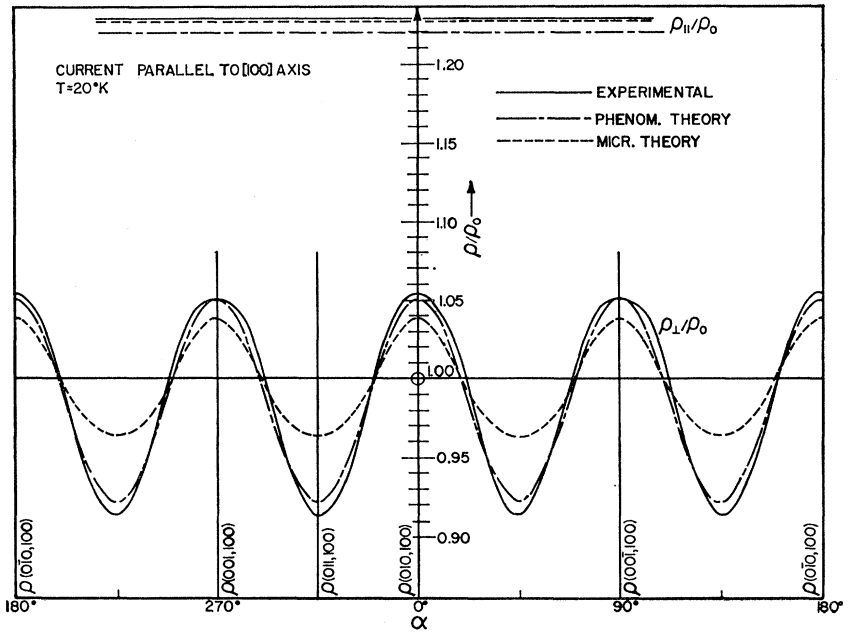

FIG. 6. Resistivity of a ⟨100⟩ sample in a transverse or longitudinal field, as calculated by the phenomenological theory of Döring, and by the microscopic theory (delta model) with hyperbolic saturation curve. The experimental data at 20°K are shown by the solid curve.

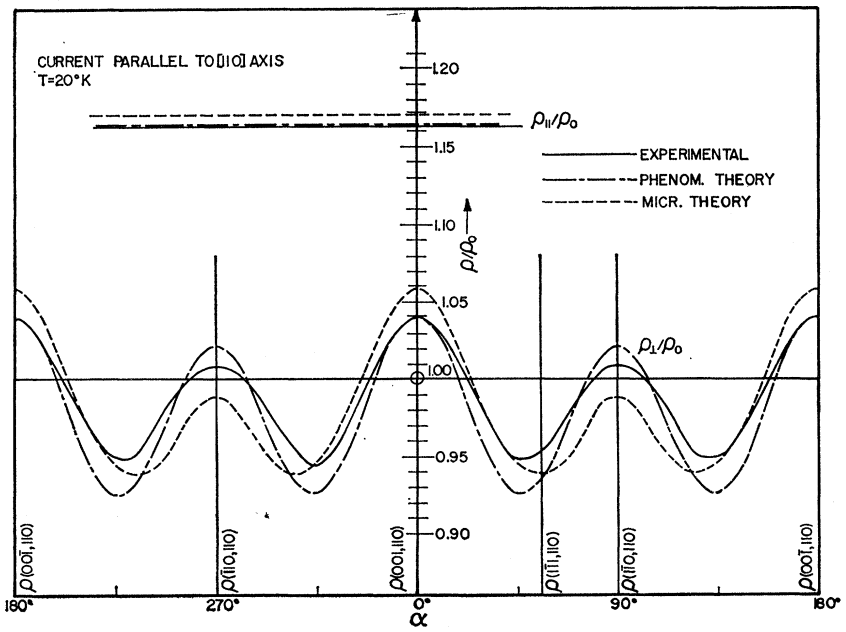

FIG. 7. Resistivity of a ⟨110⟩ sample in a transverse or longitudinal field, as calculated by the phenomenological theory of Döring, and by the microscopic theory (delta model) with the hyperbolic saturation curve. The experimental data at 20°K are shown by the solid curve.

Table III) are also shown on Figs. 6 and 7, for comparison.

Since $b<e$, spin-orbit interaction decreases the probability of being scattered into a state of the pair, in this delta model. Since q is of order unity, we see that the degenerate pairs are responsible for the major part of the observed resistivity of the alloy, and the background of states for only α minor part.

XII. RELATION BETWEEN PHENOMENOLOGICAL THEORY AND DELTA MODEL

For qualitative purposes, the relation between the Döring coefficients and the shape of the saturation curve may be seen by expanding C in powers of $(\alpha)_j^2$;

$$C=qC_0(1+B_2(\alpha)_j^2+B_4(\alpha)_j^4+\cdots). \quad (12)$$

If we neglect B_6, $B_8\cdots$, then Eq. (12) together with Eqs. (7), (8), and (11) lead in the delta model to an expression for $\rho(\alpha, \beta)$ which reduces exactly to the form proposed by Döring [Eq. (1)], with the following values of the coefficients:

$$k_1=(-2qpB_2+A_2)/T,$$
$$k_2=A_2/T,$$
$$k_3=-4qB_4(1-\tfrac{1}{3}p)/T,$$
$$k_4=-2qpB_4/T,$$
$$k_5=0,$$
$$(T=2q(1-\tfrac{1}{3}p)(3+B_2+\tfrac{1}{3}B_4)+1+\tfrac{1}{3}A_2). \quad (13)$$

We have by definition $q\geq 0$. A saturation curve of the type shown on Fig. 5 gives $B_2<0$ and $B_4>0$. Then, with $A_2>0$ and $0\leq p\leq 1$ as the only assumptions, we can see that the Eqs. (13) give $k_1>0$, $k_2>0$, $k_1\geq k_2$, $k_3\leq 0$, $k_4\leq 0$, in good agreement with our experimental data (Table III) at 20°K. The only discrepancy is with k_5, predicted to vanish.

Moreover, Eqs. (13) show that the nonlinearity of the saturation curve is essential. If we were to assume $B_4=0$, this would imply $k_3=k_4=0$. Then the $\rho_\perp/\rho_0$ curve for the ⟨100⟩ sample would be predicted to be straight and horizontal, in disagreement with the experimental curve (Fig. 6). Actually, k_3 and k_4 are as large as k_1 and k_2.

In practice, the coefficients B_6 and B_8 in Eq. (12) are too large to be neglected, and the preceding discussion has only qualitative validity.

XIII. LAMBDA MODEL

Apart from the delta model of Fig. 4, we have also investigated a model where the dominant orbital magnetic vectors are of four different types ($j=1, 2, 3, 4$), each of them parallel to one of the four equivalent ⟨111⟩ axes of the crystal.

We have fitted this "lambda model" to the experimental data at 20°K, using the hyperbolic saturation curve of Eq. (10), and using Eqs. (7), (8), and (11), as before. The best fit corresponds to the second line of Table V. Note that $b>e$, so that mixing here increases the scattering rate.

The delta model and the lambda model may be considered as two extreme, but opposite, cases among all possible models consistent with cubic symmetry. It is likely that intermediate, more complicated models would give intermediate results.

XIV. $L_xS_x+L_yS_y$ SATURATION THEORY

The theory presented here needs only a slight modification in order to apply to the case where the mixing of two near-degenerate states is due to the other part $A(L_x'S_x'+L_y'S_y')$ of spin-orbit interaction. Consider a pair of states ψ_a and ψ_b of opposite spin, having the orbital magnetic vector $\mathbf{m}_j$ as defined by Eq. (5). Then one can show

$$|\langle\psi_a|A(L_x'S_x'+L_y'S_y')|\psi_b\rangle|^2=|\tfrac{1}{2}iA\hbar|^2|\mathbf{m}|^2 \times(1-(\alpha)_j^2). \quad (14)$$

Hence, as before, the degree of mixing between the two states depends only on the value of the component $(\alpha)_j$ of the magnetization α along $\mathbf{m}_j$. The only difference is that the mixing now is zero for $(\alpha)_j^2=1$ and increases (with a tendency to saturation) when $(\alpha)_j^2$ decreases to zero. The hyperbolic saturation curve of Eq. (10), for example, should now be written:

$$C=qC_0\frac{1+b'[1-(\alpha)_j^2]}{1+e'[1-(\alpha)_j^2]}. \quad (15)$$

This new saturation curve is related to the type of curves shown on Fig. 5 by a left-right mirror reflection. Note that the most important characteristics of the saturation curve, namely, its concavity (either up or down), is invariant under the reflection.

Assuming the delta model, we have fitted Eq. (15) to the data at 20°K, using Eqs. (7), (8), and (11). The best fit corresponds to the third line of Table V; since $b'<e'$, mixing by the $A(L_x'S_x'+L_y'S_y')$ interaction decreases the scattering rate.

We have also fitted Eq. (15) to the data with the lambda model, using Eqs. (7), (8), and (11). Here the best fit corresponds to the fourth line of Table V. Since $b'>e'$, mixing increases C and the scattering rate.

As shown by Smit,[12] the Born approximation gives here a nonzero result, and it is not entirely necessary to use the Slater-Koster approximation or other approximations in order to derive a saturation curve from first principles.

Since the spin-down $3d$ states are probably completely filled in our alloy, the only near degeneracy which may be significant with the present spin-flip perturbation $A(L_x'S_x'+L_y'S_y')$ must be between spin-up $3d$ states

and spin-down 4s states; the mixing will be possible if these 4s states have partial 3d character.

XV. FINAL REMARKS

We have fitted our theory to the experimental data in four different cases. The quality of the fit may be expressed in each case by giving the root-mean-square difference between theoretical and experimental values of resistivity. The rms difference obtained by sampling over 12 selected directions of the magnetization or current is listed in the last column of Table V, in arbitrary units. We see that the best fits are obtained with the delta model in the case of the $A(L_x'S_x'+L_y'S_y')$ interaction, and with the lambda model in the case of the $AL_z'S_z'$ interaction, and they are almost equally good. Even though not the best, the delta model in the $AL_z'S_z'$ case is still fairly successful, as was shown in Figs. 6 and 7.

The main advantage of our microscopic theory is that it formulates all spin-orbit properties of the scattering impurity in terms of an orbital magnetic vector and of a saturation curve, without having to specify further the state of the 3d electrons. Nevertheless, one may try to locate the near-degenerate states in existing calculated band structures for pure nickel. As mentioned before,[20] the proximity of critical points may enhance the effect of accidental degeneracies; the points X and L are possible candidates.[25] Unfortunately, the strong impurity potential modifies considerably the wavefunction on the impurity, and it is not obvious that these pure metal calculations are of much meaning for our problem. This is also shown by the fact that we found the Born approximation to be inadequate for our scattering calculations in the $AL_z'S_z'$ case. Moreover, in a disordered alloy, it is not certain that spin-orbit interaction would mix together only states of same $\mathbf{k}$. If the $\mathbf{k}$ selection rule is broken, then a much wider class of degeneracies becomes active in the alloy.

Judging solely from the point of view of $\mathbf{m}_j$ directions, pairs made of a state of type Δ_2 and of a state of type Δ_2' would be one suitable choice for the delta model since the $\mathbf{m}_j$ of such pairs are parallel to the fourfold Δ directions. However, at least in the case of pure nickel, the Δ_2' states are far below the Fermi level.

An orbital magnetic vector can be defined only for a pair of states. Therefore, the present theory does not apply to the case of a degenerate triplet.

We note, finally, that it cannot be excluded that the nonlinearities giving rise to the coefficients k_3, k_4, and k_5 might come from another source than the existence of near degeneracies. Such a source may be the failure of Eq. (7a) in the presence of multiband conduction or of anisotropic mean free path.

[25] After the manuscript of the present paper had been written, there appeared an interesting abstract by W. N. Furey, Bull. Am. Phys. Soc. **12**, 311 (1967). It stresses the importance of near-degeneracies in determining the magnetocrystalline anisotropy of pure nickel, as calculated from an "interpolated" band structure. The near-degeneracy would be located in a limited region around point X. As in our case, the higher-order phenomenological coefficient (there called K_2) is of the same order or magnitude as K_1, because of the degeneracy.

XVI. CONCLUSIONS

The Döring coefficients k_1–k_5 of our 15% Fe–85% Ni single crystal have been determined at 20, 77, and 299°K, by fitting of the phenomenological Döring expression to the experimental data of resistivity in a magnetic field. By using an expression based on Matthiessen's rule, it is possible to extrapolate the values of the Döring coefficients to the case of impurity scattering alone and to the case of phonon scattering alone. The coefficients are large and positive in the first case, and are small or slightly negative in the second case.

A simple microscopic theory has been developed, which is able to reproduce correctly most qualitative features of the single-crystal data. The first assumption made in this theory is that conduction electrons are impurity-scattered into near-degenerate 3d states, present at the Fermi level of the alloy. The second assumption is that the "orbital magnetic vectors," which indicate how spin-orbit interaction AL_zS_z affects these orbital 3d states, have special crystal directions. These directions may either be parallel to the fourfold cubic axes (delta model) or to the threefold cubic axes (lambda model). The third assumption is that, because of the near degeneracy, the effect of spin-orbit interaction on a state is large and nonlinear, and tends to saturate at a constant maximum value; first-order perturbation theory is insufficient.

The theory is extended to cover the case where the $A(L_x'S_x'+L_y'S_y')$ interaction is the mixing agent between near-degenerate states. A reasonable fit to the experimental data may be achieved here too.

We have shown that, whatever interaction is assumed to be active, the best fit always requires that the mixing increase the scattering rate in the lambda model, and decrease it in the delta model. [*Note added in proof.* L. Hodges, D. R. Stone, and A. V. Gold [Phys. Rev. Letters **19**, 655 (1967)] have recently shown that the spin-orbit parameter of nickel metal is $A\hbar^2=0.102$ eV instead of 0.075 eV. This would cause a proportional increase of the band gap values Δ quoted for the various saturation curves on our Fig. 5.]

ACKNOWLEDGMENTS

We would like to express our gratitude to Professor J. H. Nee for the glue used to hold the samples during preparation. George Schnakenberg performed certain of the measurements of resistivity. Dr. V. Folen and Dr. J. Schelleng kindly provided a description of an x-ray crystal orientation machine. Many numerical calculations were performed at the Carnegie Institute of Technology Computation Center.